Supplementary Information (SI) for Materials Advances.

Supporting Information

Scalable, epitaxy-preserving transfer of freestanding perovskite and layered oxide membranes with tunable strain

Habib Rostaghi Chalaki,[a] Ebenezer Seesi,[a] Avari Suber,[a] Sang-Hoon Nam,[b] Yo-Han Suh,[c] and Dongkyu Lee[a,*]

[a]Department of Mechanical Engineering, University of South Carolina, Columbia, SC 29208, USA

[b]Research Laboratory of Electronics, Massachusetts Institute of Technology, Cambridge, MA 02139

[c]Smart Electronics Research Center, Korea Electronics Technology Institute(KETI), Jeonju 54853, Republic of Korea

Lattice parameter and strain calculations

The out-of-plane lattice parameter (*c*) of the films was determined from the d-spacings of symmetric (00l) reflections. Specifically, c_{film} values calculated from the (004) and (008) peak positions were averaged. The in-plane lattice parameter (*a*) was determined from reciprocal space maps (RSMs) by fitting the peak-center positions (q_x and q_z) for epitaxially related *hkl* reflections from both the substrate and the film. The extracted q_x values were used to calculate a_{film} according to

$$a_{\mathrm{film}} = \left[\frac{\left(\frac{q_{\mathrm{x\,(sub)}}}{\mathrm{h}_{\mathrm{sub}}}\right)}{\left(\frac{q_{\mathrm{x\,(film)}}}{\mathrm{h}_{\mathrm{film}}}\right)}\right] \times a_{\mathrm{sub}} \tag{1}$$

, which reduces to $a_{\mathrm{film}} = (q_{\mathrm{x,sub}} / q_{\mathrm{x,film}}) \times a_{\mathrm{sub}}$ when the same in-plane index is used for the film and substrate peak.

The in-plane strain was calculated as

$$\varepsilon = \frac{a_{\mathrm{film}} - a_{\mathrm{bulk}}}{a_{\mathrm{bulk}}} \times 100\% \tag{2}$$

The same procedure was used to determine the in-plane lattice parameter of the SCAO sacrificial layer, a_{SCAO}, enabling identification of whether the film was coherently strained to the sacrificial layer ($q_{\mathrm{x,film}} \approx q_{\mathrm{x,SCAO}}$) and whether the sacrificial layer remained strained to the substrate ($q_{\mathrm{x,SCAO}} \approx q_{\mathrm{x,sub}}$).

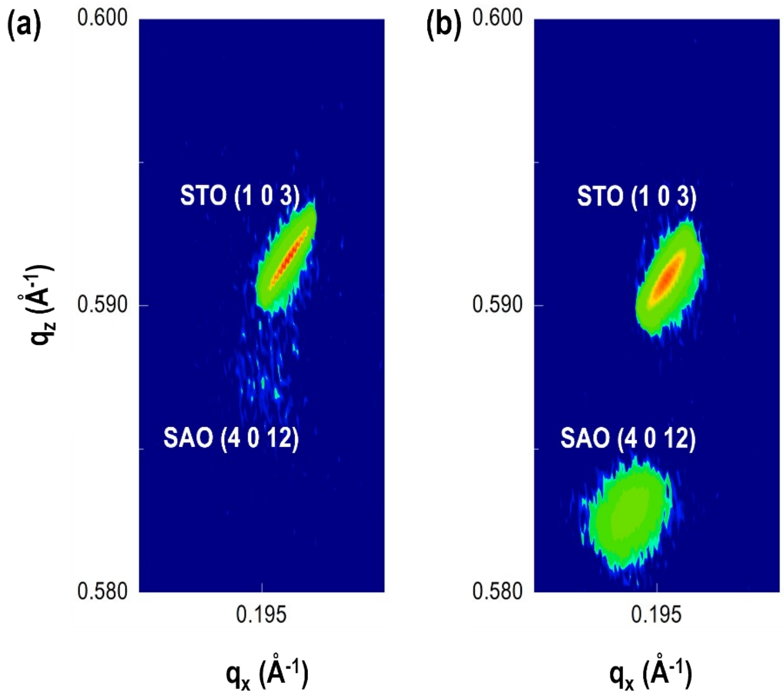

Figure S1. Representative XRD RSMs around the substrate STO (103) reflection for SAO layers grown epitaxially on STO. (a) 30 nm-thick SAO and (b) 120 nm-thick SAO.

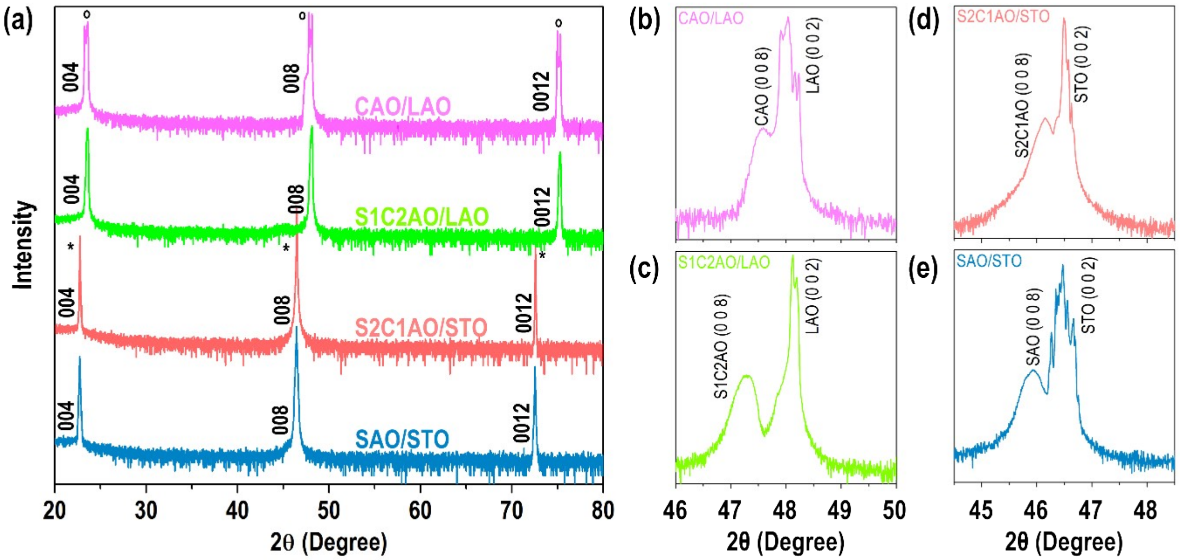

Figure S2. **X-ray diffraction analysis of epitaxial SCAO sacrificial layears.** (a) Out-of-plane θ-2θ scans of SCAO sacrificial layers grown epitaxially on STO and LAO substrates. The * and o symbols denote the STO and LAO (00*l*) peaks, respectively. (b-d) Magnified θ-2θ scans around the substrate (002).

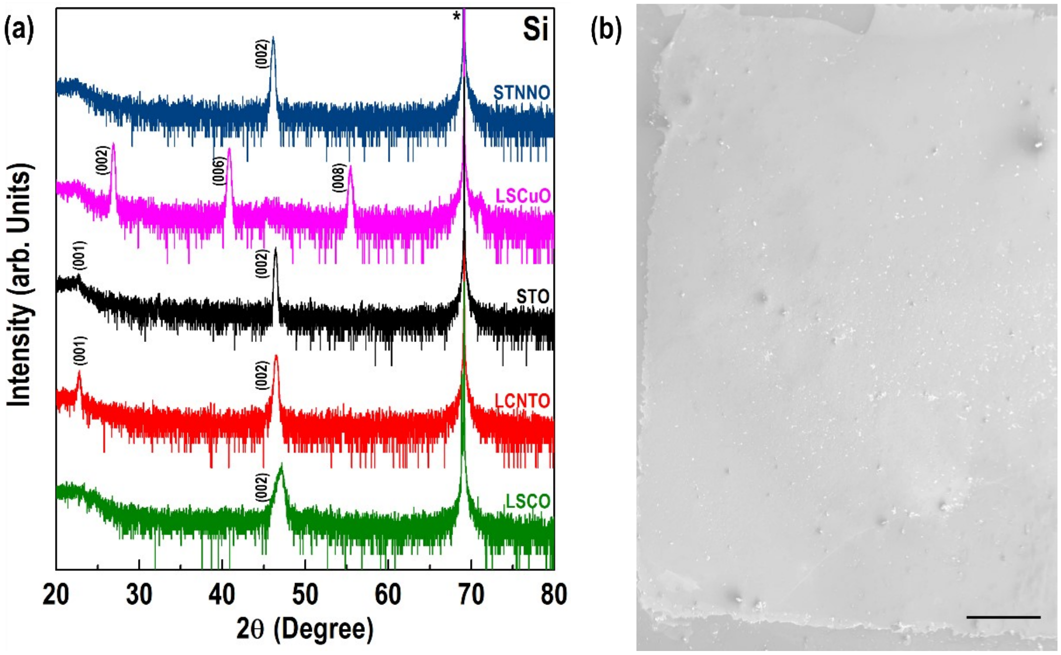

Figure S3. **Structural characterization of transferred oxide membranes on Si.** (a) Out-of-plane *θ–2θ* scans of LSCO, LCNTO, STO, LSCuO, and STNNO membranes transferred onto Si. Well-defined (00*l*) reflections from each membrane confirm retention of the epitaxial out-of-plane orientation after transfer. (b) Representative SEM image of a transferred STO membrane on Si, demonstrating large-area transfer with high uniformity and minimal visible surface defects. Scale bar: 500 μm.

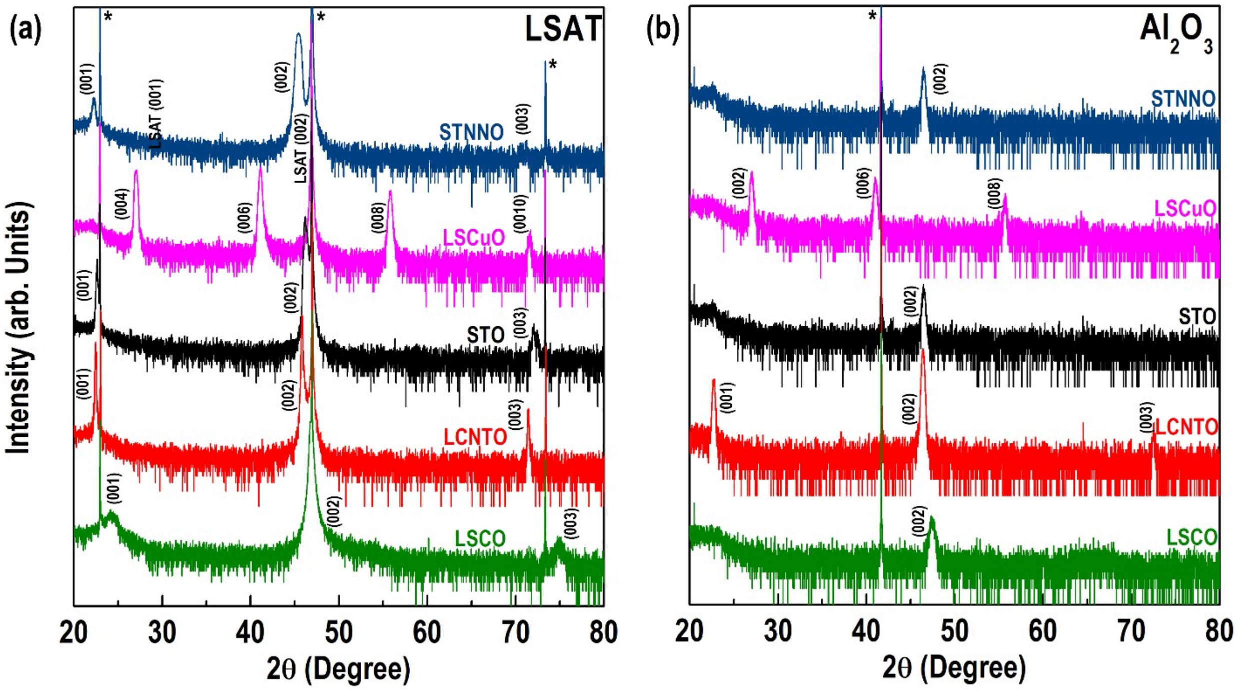

Figure S4. **X-ray diffraction analysis of epitaxial reference films and transferred oxide membranes.** (a) Out-of-plane *θ-2θ* scans of relaxed epitaxial STNNO, LSCuO, STO, LCNTO, and LSCO layers grown on LSAT substrates. (b) Out-of-plane *θ–2θ* scans of STNNO, LSCuO, STO, LCNTO, and LSCO membranes transferred onto sapphire. The * symbol indicates substrate (00*l*) reflections.

Table S1. Lattice mismatch between the sacrificial layers and the substrate materials.

Sacrificial layer	a_{bulk} (Å)	Thickness (nm)	Substrate (Å)	Lattice mismatch (*a*-*b* plane)	In-plane strain (%)
$Sr_3Al_2O_6$ (SAO) [1]	3.961	120	STO, a = 3.904 [2]	~ -1.5 %	0
	3.961	30	STO, a = 3.904	~ -1.5 %	-1.46
$Sr_2CaAl_2O_6$ (S2C1AO) [3]	3.907	120	STO, a = 3.904	~ 0.1 %	0.07
$SrCa_2Al_2O_6$ (S1C2AO) [4]	3.852	30	LAO, a = 3.780 [5]	~ -1.9 %	-1.89
$Ca_3Al_2O_6$ (CAO) [6]	3.819	120	LAO, a = 3.780	~ -1.1 %	-1.03

Table S2. Lattice mismatch between the films and strain-controlled sacrificial layers.

Materials	a_{bulk} (Å)	c_{bulk} (Å)	Sacrificial layer (Å)	Sub.	In-plane strain (%)
$Sr_{0.95}Ti_{0.76}Ni_{0.05}Nb_{0.19}O_3$ (STNNO) [7, 8]	3.941	3.941	Relaxed SAO a = 3.961	STO	0.5
$La_{0.7}Ca_{0.2}Ni_{0.25}Ti_{0.75}O_3$ (LCNTO) [9, 10]	3.924	3.924	Relaxed S2C1AO a = 3.907	STO	-0.5
$SrTiO_3$ (STO) [2]	3.904	3.904	Strained SAO a = 3.904	STO	0
$La_{0.8}Sr_{0.2}CoO_3$ (LSCO) [11]	3.851	3.851	Strained S1C2AO a = 3.780	LAO	-1.87
$La_{1.85}Sr_{0.15}CuO_4$ (LSCuO) [12]	3.770	13.232	Strained CAO a = 3.780	LAO	0.26

References

1. Lu, D.; Baek, D. J.; Hong, S. S.; Kourkoutis, L. F.; Hikita, Y.; Hwang, H. Y., Synthesis of freestanding single-crystal perovskite films and heterostructures by etching of sacrificial water-soluble layers. *Nature materials* **2016,** *15* (12), 1255-1260.
2. Fuchs, D.; Adam, M.; Schweiss, P.; Gerhold, S.; Schuppler, S.; Schneider, R.; Obst, B., Structural properties of slightly off-stoichiometric homoepitaxial SrTi x O 3− δ thin films. *Journal of Applied Physics* **2000,** *88* (4), 1844-1850.
3. Yun, S.; le Cozannet, T. E.; Christoffersen, C. H.; Brand, E.; Jespersen, T. S.; Pryds, N., Strain Engineering: Perfecting Freestanding Perovskite Oxide Fabrication. *Small* **2024**, 2310782.
4. Varshney, S.; Ramis, M.; Choo, S.; Coll, M.; Jalan, B., Epitaxially grown single-crystalline SrTiO 3 membranes using a solution-processed, amorphous SrCa 2 Al 2 O 6 sacrificial layer. *Journal of Materials Chemistry C* **2024,** *12* (35), 13809-13815.
5. Boĭkov, Y. A.; Danilov, V., Electrical resistivity and magnetoresistance of nonuniformly mechanically strained films (30 nm) of the La0. 67Ca0. 33MnO3 manganite. *Physics of the Solid State* **2006,** *48* (8), 1533-1538.
6. Chiabrera, F. M.; Yun, S.; Li, Y.; Dahm, R. T.; Zhang, H.; Kirchert, C. K.; Christensen, D. V.; Trier, F.; Jespersen, T. S.; Pryds, N., Freestanding perovskite oxide films: Synthesis, challenges, and properties. *Annalen der Physik* **2022,** *534* (9), 2200084.
7. Weber, M. L.; Wilhelm, M.; Jin, L.; Breuer, U.; Dittmann, R.; Waser, R.; Guillon, O.; Lenser, C.; Gunkel, F., Exsolution of embedded nanoparticles in defect engineered perovskite layers. *ACS nano* **2021,** *15* (3), 4546-4560.
8. Hirata, S.; Ohtaki, M.; Watanabe, K., Highly improved thermoelectric performance of Nb-doped SrTiO3 due to significant suppression of phonon thermal conduction by synergetic effects of pores and metallic nanoparticles. *Ceramics International* **2020,** *46* (16, Part A), 25964-25969.
9. Kim, Y. H.; Kang, Y.; Jo, S.; Jeong, H.; Neagu, D.; Myung, J.-h., Shape-shifting nanoparticles on a perovskite oxide for highly stable and active heterogeneous catalysis. *Chemical Engineering Journal* **2022,** *441*, 136025.
10. El Loubani, M.; Yang, G.; Kouzehkanan, S. M. T.; Oh, T.-S.; Balijepalli, S. K.; Lee, D., Influence of redox engineering on the trade-off relationship between thermopower and electrical conductivity in lanthanum titanium based transition metal oxides. *Materials Advances* **2024,** *5* (22), 9007-9017.
11. Lee, D.; Lee, Y.-L.; Grimaud, A.; Hong, W. T.; Biegalski, M. D.; Morgan, D.; Shao-Horn, Y., Enhanced Oxygen Surface Exchange Kinetics and Stability on Epitaxial La0.8Sr0.2CoO3−δ Thin Films by La0.8Sr0.2MnO3−δ Decoration. *The Journal of Physical Chemistry C* **2014,** *118* (26), 14326-14334.
12. Zhu, J.; Zhao, Z.; Xiao, D.; Li, J.; Yang, X.; Wu, Y., Characterization and catalytic activity in NO decomposition of La2− xSrxCuO4 (0≤ x≤ 1) compounds with T* phase structure. *Materials Chemistry and Physics* **2005,** *94* (2-3), 257-260.